ON THE CHOICE OF PRIMARY VARIABLES IN TRANSIENT GEOTHERMAL WELLBORE MODELLING

Ryan Tonkin[1], John O'Sullivan[1], Michael O'Sullivan[1]

[1] Department of Engineering Science, University of Auckland, Auckland, New Zealand

rton671@aucklanduni.ac.nz

Keywords: *wellbore, multi-feed, transient, two-phase, simulation, finite volume method, primary variables*

ABSTRACT

Transient flow in a geothermal wellbore is modelled using equations for conservation of mass, momentum and energy. Additional constitutive equations that describe phase slip, heat transfer and frictional effects are also required for model closure. The transient wellbore simulator described in this paper solves discrete two-phase conservation equations numerically using the Newton-Raphson procedure. Additionally, the constitutive equation describing phase slip is included in the set of equations to be solved implicitly. This method requires four primary variables, however, the best choice of the primary variables is not clear. This paper discusses the use of different combinations of primary variables in our transient geothermal wellbore simulator. The numerical performance of each model is assessed using a set of problems that have been developed to test the transient simulator. This suite of test problems covers a range of operating conditions and serves as a benchmark for future simulator development. It was found that using pressure, temperature (swapped with saturation for two-phase conditions), vapour velocity and liquid volume flux resulted in the best numerical performance for all cases tested.

1. INTRODUCTION

Geothermal wellbore simulators numerically solve the equations for conservation of mass, momentum and energy. These conservation equations are typically solved for three primary variables that are required to completely specify the thermodynamic state of the wellbore (Pan et al., 2014). Table 1 gives the primary variables used in past transient geothermal wellbore simulators. Three of the four simulators use persistent primary variables, where the primary variables remain the same for all phase states. Pan et al.'s (2011) simulator T2WELL solves a second conservation of mass equation to account for CO_2 and is the only simulator to use primary variable switching. In this case, temperature, T, is used for single phase flow but is swapped to vapour saturation, S_v, for two-phase conditions.

Table 1: Primary variables used in past transient geothermal wellbore simulators

Model				
WELLBORE (Miller, 1980)	P	Q_m	e_{mix}	$-$
Garcia-Valladares et al. (2006)	P	Q_m	h_{fmix}	$-$
T2WELL (Pan et al., 2011)	P	u_{mix}	$T(S_v)$	x_{CO2}
Akbar et al. (2016)	P	u_{mix}	h_{mix}	$-$

In Table 1, P is pressure, Q_m is total mass flow, u_{mix} is mass weighted mixture velocity, and x_{CO2} is the mass fraction of CO_2. The variables e_{mix} and h_{mix} are the static (mass weighted) internal energy and enthalpy, respectively, and h_{fmix} is the flowing (mass flux weighted) enthalpy.

A different approach was taken when formulating our wellbore model. A fourth equation, the constitutive model for slip was added to the three conservation equations and is also solved implicitly. Solving the slip equation in this way provides implicit knowledge of the flow direction for both phases. This is beneficial for upwinding procedures that are required for numerical stability. Additionally, in some cases, three equation models do not allow the empirical slip parameters to be calculated explicitly. This makes assessing wellbore simulator performance (e.g. data matching, convergence and time stepping) difficult when different slip models and primary variable combinations are used.

Solving the slip equation implicitly requires a fourth primary variable. Therefore, none of the primary variable combinations presented in Table 1 are appropriate. Only one previous simulator, a steady-state simulator by Tachimori (1982), has solved the slip equation implicitly. They used P, $T(S_v)$, u_v and u_l as primary variables. These variables were initially used in our simulator, however, after several issues were encountered (discussed further in this paper), two other choices for primary variables were explored. This paper discusses how these three formulations were implemented and compares their performance on eight test problems.

2. TWO-PHASE CONSERVATION EQUATIONS

Transient flow in geothermal wells is modelled by considering the conservation of mass, momentum and energy. A three-equation model, that describes the fluid as a mixture rather that each phase individually, is given in (1), (2) and (3) below (Pan et al., 2011, Tonkin et al. 2020, Yadigaroglu, 2018).

The conservation of mass for a two-phase fluid mixture is

$$\frac{\partial}{\partial t}[\rho_l S_l + \rho_v S_v] +$$
$$\frac{1}{A}\frac{\partial}{\partial s}[A\rho_l S_l u_l + A\rho_v S_v u_v] - q_{mass} = 0. \quad (1)$$

Here, ρ_β is the density, S_β is the saturation and u_β is the velocity of phase $\beta = v, l$. The subscripts v and l represent the vapour and liquid phases, respectively. The mass exchange between the reservoir and the wellbore is modelled by the source term q_{mass}.

The conservation of momentum is

$$\frac{\partial}{\partial t}[\rho_l S_l u_l + \rho_v S_v u_v] + \frac{1}{A}\frac{\partial}{\partial s}[A\rho_l S_l u_l^2 + A\rho_v S_v u_v^2]$$
$$+\frac{\partial P}{\partial s} + \frac{2}{R}\tau + (\rho_l S_l + \rho_v S_v)g\frac{\partial z}{\partial s} - q_{mom} = 0. \quad (2)$$

Here, P is pressure, g is gravity, z is vertical depth and s is the distance along the wellbore. Wellbore friction, τ, is defined by a constitutive model, discussed in the companion paper by Tonkin et al. (2020).

The conservation of energy for a two-phase mixture is

$$\frac{\partial}{\partial t}\left[\rho_l S_l\left(h_l+\frac{u_l^2}{2}\right)+\rho_v S_v\left(h_v+\frac{u_v^2}{2}\right)-P\right]+$$

$$\frac{1}{A}\frac{\partial}{\partial s}\left[A\rho_l S_l u_l\left(h_l+\frac{u_l^2}{2}\right)+A\rho_v S_v u_v\left(h_v+\frac{u_v^2}{2}\right)\right]+$$

$$(\rho_l S_l u_l+\rho_v S_v u_v)g\frac{\partial z}{\partial s}+q_{heat}-q_{ener}=0. \qquad (3)$$

Here, h_β is specific enthalpy, q_{heat} models wellbore heat transfer and q_{ener} models energy transfer due to mass exchange with the reservoir.

Three equation models for two-phase flow require an additional constitutive equation to model phase slip. This simulator uses the drift flux model originally presented by Zuber and Findlay (1965) and used in some past transient simulators. Pan et al. (2011) solved equations (4) and (5) for the phase velocities while Garcia-Valladares et al. (2006) and Akbar et al. (2016) solved the drift flux model for vapour saturation.

The vapour and liquid velocities are calculated using the drift flux model using:

$$u_v = C_0 F_V + u_d, \qquad (4)$$

and

$$u_l = \frac{1-S_v C_0}{1-S_v} F_V - \frac{S_v}{1-S_v} u_d. \qquad (5)$$

In (4) and (5), F_V is the total volume flux defined as,

$$F_V = S_l u_l + S_v u_v. \qquad (6)$$

The distribution coefficient, C_0, accounts for non-uniform saturation and volume flux profiles across the well while the drift velocity, u_d accounts for the relative velocity between phases caused by buoyancy forces (Yadigaroglu, 2018). Pan et al.'s (2011) constitutive model for C_0 and u_d (adapted from Shi et al. (2005)) is used in this simulator.

The constitutive equations for friction, τ, heat transfer, q_{heat}, and for evaluating sources q_{mass}, q_{mom} and q_{ener} are discussed in a companion paper (Tonkin et al.,2020).

3. NUMERICAL IMPLEMENTATION

An analytical solution of the non-linear equations for mass, momentum and energy conservation is not possible and they must be solved numerically. To do this, the governing equations presented in Section 2 are discretised and solved for the primary thermodynamic variables using the Newton-

Raphson method. An outline of this numerical method is given in Section 3.5.

Three different primary variable combinations, given in Table 2, are tested in this work. Two of the primary variables remain the same for all three cases. For single-phase flow, pressure and temperature are used. They are switched to pressure and vapour saturation for two-phase conditions. These primary variables are the standard choice when simulating geothermal reservoirs using the pure water equation of state and have proven to be a very robust method for dealing with multi-phase systems (Pruess et al., 2012, Croucher, 2020).

The two remaining primary variables are flow variables and appear predominantly in the momentum equation, as such we will refer to them as flowing primary variables. Three different options for the flowing primary variables were tested. These were the phase velocities, phase volume fluxes and a mixed formulation that used the vapour velocity and liquid volume flux.

Table 2: Primary variables tested in this work

Velocity formulation	P	$T(S_v)$	u_v	u_l
Volume flux formulation	P	$T(S_v)$	F_{Vv}	F_{Vl}
Mixed formulation	P	$T(S_v)$	u_v	F_{Vl}

3.1 Discrete conservation equations

A fully implicit, one-dimensional finite volume discretisation is used in this simulator. Here, static wellbore properties, e.g. pressure, temperature and saturation, are defined at the centre of each wellbore element, as shown in Figure 1, and flowing variables, e.g. phase velocities and fluxes, are defined on the interface between elements, as shown in Figure 2.
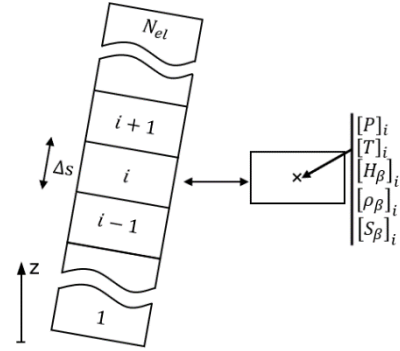

Figure 1: Discretisation scheme for the mass and energy equations centred on element i

The discrete conservation of mass and energy are given in (7) and (8) below for a generic element i. Here, the superscripts $n+1$ and n indicate the current and previous time steps, respectively. The subscript i is the spatial index of an element centre. The subscript $i+1/2$ is the index of the interface between elements i and $i+1$.

$$\frac{1}{\Delta t}\left([S_v\rho_v+S_l\rho_l]_i^{n+1}-[S_v\rho_v+S_l\rho_l]_i^n\right)+\frac{1}{[V]_i}\left([AF_{mv}+AF_{ml}]_{i+1/2}^{n+1}-[AF_{mv}+AF_{ml}]_{i-1/2}^{n+1}\right)-[q_{mass}]_i^{n+1}=0 \qquad (7)$$

$$\frac{1}{\Delta t}\left([S_v\rho_v H_v+S_l\rho_l H_l-P]_i^{n+1}-[S_v\rho_v H_v+S_l\rho_l H_l-P]_i^n\right)+\frac{1}{[V]_i}\left([AF_{mv}H_v+AF_{ml}H_l]_{i+1/2}^{n+1}-[AF_{mv}H_v+AF_{ml}H_l]_{i-1/2}^{n+1}\right)+$$

$$[q_{heat}]_i^{n+1}+[F_{mv}+F_{ml}]_i^{n+1}g\frac{z_{i+1}-z_{i-1}}{s_{i+1}-s_{i-1}}-[q_{ener}]_i^{n+1}=0 \qquad (8)$$

$$\frac{1}{\Delta t}\left([F_{mv}+F_{ml}]_{i+1/2}^{n+1/2}-[F_{mv}+F_{ml}]_{i+1/2}^{n}\right)+$$

$$\frac{1}{[V]_{i+\frac{1}{2}}}\begin{cases}[AF_{mv}u_v]_{i+1/2}^{n+1}-[AF_{mv}u_v]_{i-1/2}^{n+1}, & [X_v]_{i+1/2}^{n+1}\geq 0 \\ [AF_{mv}u_v]_{i+3/2}^{n+1}-[AF_{mv}u_v]_{i+1/2}^{n+1}, & [X_v]_{i+1/2}^{n+1}< 0\end{cases}+\frac{1}{[V]_{i+\frac{1}{2}}}\begin{cases}[AF_{ml}u_l]_{i+1/2}^{n+1}-[AF_{ml}u_l]_{i-1/2}^{n+1}, & [X_l]_{i+1/2}^{n+1}\geq 0 \\ [AF_{ml}u_l]_{i+3/2}^{n+1}-[AF_{ml}u_l]_{i+1/2}^{n+1}, & [X_l]_{i+1/2}^{n+1}< 0\end{cases}$$

$$+\frac{P_{i+1}^{n+1}-P_i^{n+1}}{s_{i+1}-s_i}+\frac{2}{R}\tau_{i+1/2}^{n+1}+[\rho_v S_v+\rho_l S_l]_{i+1/2}^{n+1}g\frac{z_{i+1}-z_i}{s_{i+1}-s_i}-[q_{mom}]_{i+1/2}^{n+1}=0 \qquad (16)$$

The time step is Δt and the volume of a wellbore block is $[V]_i$, defined as

$$[V]_i=[A]_i\Delta s_i \qquad (9)$$

where $[A]_i$ is the average cross-sectional area and Δs_i is the axial length of a wellbore element.

The mass flux of a phase on an interface is defined as

$$[F_{m\beta}]_{i+1/2}^{n+1}=[\rho_\beta S_\beta]_{i+1/2}^{n+1}[u_\beta]_{i+1/2}^{n+1}. \qquad (10)$$

The interface saturation and density are weighted according to the direction of the flow. This is called upstream weighting or upwinding. The interface saturation is calculated using:

$$[S_\beta]_{i+1/2}^{n+1}\begin{cases}[S_\beta]_i^{n+1}, & [X_\beta]_{i+1/2}^{n+1}\geq 0 \\ [S_\beta]_{i+1}^{n+1}, & [X_\beta]_{i+1/2}^{n+1}< 0\end{cases}, \qquad (11)$$

and the interface density is calculated using:

$$[\rho_\beta]_{i+1/2}^{n+1}\begin{cases}[\rho_\beta]_i^{n+1}, & [X_\beta]_{i+1/2}^{n+1}\geq 0 \\ [\rho_\beta]_{i+1}^{n+1}, & [X_\beta]_{i+1/2}^{n+1}< 0\end{cases}. \qquad (12)$$

Here, $[X_\beta]_{i+1/2}^{n+1}$ refers to the flowing primary variable of a phase.

The calculation of phase velocity, $[u_\beta]_{i+1/2}^{n+1}$, differs depending on which primary variables are used. Its calculation is outlined in Sections 3.2, 3.3 and 3.4 for the velocity, volume flux and mixed formulations, respectively.

In (8), $[H_\beta]_i^{n+1}$ is the sum of enthalpy and kinetic energy of each phase,

$$[H_\beta]_i^{n+1}=[h_\beta]_i^{n+1}+[E_{K\beta}]_i^{n+1} \qquad (13)$$

where $[E_{K\beta}]_i^{n+1}$ is the average kinetic energy of a phase. It is defined as the average of the kinetic energy at the interfaces,

$$[E_{K\beta}]_i^{n+1}=\frac{1}{2}\left(\frac{1}{2}[u_\beta^2]_{i+1/2}^{n+1}+\frac{1}{2}[u_\beta^2]_{i-1/2}^{n+1}\right). \qquad (14)$$

The interface enthalpies are upstream weighted, such that

$$[H_\beta]_{i+1/2}^{n+1}\begin{cases}[H_\beta]_i^{n+1}, & [X_\beta]_{i+1/2}^{n+1}\geq 0 \\ [H_\beta]_{i+1}^{n+1}, & [X_\beta]_{i+1/2}^{n+1}< 0\end{cases}. \qquad (15)$$

The discrete momentum equation, given in (16) above, is centred on the block interface at $i+1/2$. The momentum control element is shown in red in Figure 2. Definitions of the momentum flux would be required at i and $i+1$ if a central differencing scheme was used. Instead, upwinding based on the direction of the flowing primary variables at $i+1/2$ is used.
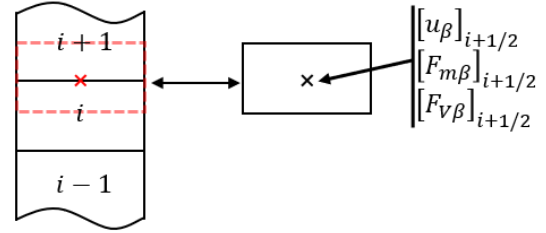

Figure 2: Discretisation scheme for the momentum equation centred on element $i+1/2$

The gravity term in (16) uses the average density on the interface,

$$[\rho_v S_v+\rho_l S_l]_{i+1/2}^{n+1}=$$
$$\frac{1}{2}\left([\rho_v S_v+\rho_l S_l]_i^{n+1}+[\rho_v S_v+\rho_l S_l]_{i+1}^{n+1}\right). \qquad (17)$$

Equation (17) must be used instead of the upwinded saturations and densities. This is because in simulations with low mass flow the liquid velocity can flip between positive and negative values after each newton iteration. This causes the value of the gravity term to change and can result in slow, and sometimes failed, convergence.

The effective interface volume, $[V]_{i+1/2}$, is the average volume of the surrounding elements:

$$[V]_{i+1/2}=\frac{1}{2}([V]_{i+1}+[V]_i). \qquad (18)$$

3.2 Velocity formulation

The velocity formulation calculates the vapour and liquid velocities, $[u_v]_{i+1/2}^{n+1}$ and $[u_l]_{i+1/2}^{n+1}$, as flowing primary variables. The phase volume flux is calculated from the phase velocity using

$$[F_{V\beta}]_{i+1/2}^{n+1}=[S_\beta]_{i+1/2}^{n+1}[u_\beta]_{i+1/2}^{n+1}, \qquad (19)$$

where the interface saturation is given in (11).

The average velocity at i is the average of the interface velocities, calculated as

$$[u_\beta]_i^{n+1}=\frac{1}{2}\left([u_\beta]_{i+1/2}^{n+1}+[u_\beta]_{i-1/2}^{n+1}\right). \qquad (20)$$

This allows the average mass flux, used in (8), to be calculated as

$$[F_{m\beta}]_i^{n+1} = [\rho_\beta S_\beta]_i^{n+1} [u_\beta]_i^{n+1}. \tag{21}$$

The slip constitutive equation is solved implicitly. For $[S_v]_{i+1/2}^{n+1} \leq 0.8$, the discrete form of (4) is solved:

$$[u_v]_{i+\frac{1}{2}}^{n+1} - [C_0]_{i+\frac{1}{2}}^{n+1} [F_V]_{i+\frac{1}{2}}^{n+1} - [u_d]_{i+\frac{1}{2}}^{n+1} = 0. \tag{22}$$

For cases where $[S_v]_{i+1/2}^{n+1} > 0.8$, (5) is solved implicitly, such that

$$[u_l]_{i+\frac{1}{2}}^{n+1} - \frac{1 - [S_v C_0]_{i+\frac{1}{2}}^{n+1}}{1 - [S_v]_{i+\frac{1}{2}}^{n+1}} [F_V]_{i+\frac{1}{2}}^{n+1}$$
$$+ \frac{[S_v]_{i+\frac{1}{2}}^{n+1}}{1 - [S_v]_{i+\frac{1}{2}}^{n+1}} [u_d]_{i+\frac{1}{2}}^{n+1} = 0. \tag{23}$$

The saturation at which these equations are switched was chosen arbitrarily as 0.8.

Equation (23) suffers from division by zero errors when $[S_v]_{i+1/2}^{n+1} \approx 1$. To prevent this issue, we solve

$$[u_l]_{i+\frac{1}{2}}^{n+1} - \frac{1 - [S_v C_0]_{i+\frac{1}{2}}^{n+1}}{1 - S_{vmax}} [F_V]_{i+\frac{1}{2}}^{n+1}$$
$$+ \frac{[S_v]_{i+\frac{1}{2}}^{n+1}}{1 - S_{vmax}} [u_d]_{i+\frac{1}{2}}^{n+1} = 0, \tag{24}$$

where $S_{vmax} = 0.9999$, for cases in which $[S_v]_{i+1/2}^{n+1} > 0.9999$.

3.3 Volume flux formulation

The volume flux formulation calculates the liquid and vapour volume fluxes, $[F_{Vv}]_{i+1/2}^{n+1}$ and $[F_{Vl}]_{i+1/2}^{n+1}$, as primary variables. Phase velocities are calculated as secondary variables using the following equation:

$$[u_\beta]_{i+1/2}^{n+1} = \begin{cases} [F_{V\beta}]_{i+1/2}^{n+1} / [S_\beta]_{i+1/2}^{n+1} & , [S_\beta]_{i+1/2}^{n+1} \neq 0 \\ 0 & , [S_\beta]_{i+1/2}^{n+1} = 0 \end{cases}. \tag{25}$$

The average volume flux of an element is the average of the interface fluxes, such that

$$[F_{V\beta}]_i^{n+1} = \frac{1}{2} \left([F_{V\beta}]_{i+\frac{1}{2}}^{n+1} + [F_{V\beta}]_{i-\frac{1}{2}}^{n+1} \right). \tag{26}$$

This allows the average mass fluxes to be calculated as

$$[F_{m\beta}]_i^{n+1} = [\rho_\beta]_i^{n+1} [F_{V\beta}]_i^{n+1}, \tag{27}$$

and the average velocity as

$$[u_\beta]_i^{n+1} = \begin{cases} [F_{V\beta}]_i^{n+1} / [S_\beta]_i^{n+1} & , [S_\beta]_i^{n+1} \neq 0 \\ 0 & , [S_\beta]_i^{n+1} = 0 \end{cases}. \tag{28}$$

The volume flux formulation does not require equation switching when solving the slip constitutive equation. Instead

(22) is solved for all values of $[S_v]_{i+1/2}^{n+1}$. This procedure has advantages because it does not introduce small discontinuities as is the case with (24).

3.4 Mixed formulation

The mixed formulation uses $[u_v]_{i+1/2}^{n+1}$ and $[F_{Vl}]_{i+1/2}^{n+1}$ as flowing primary variables. The secondary variables for the vapour phase are calculated from $[u_v]_{i+1/2}^{n+1}$ as outlined in Section 3.2. The secondary variables for the liquid phase are calculated from $[F_{Vl}]_{i+1/2}^{n+1}$ as outlined in Section 3.3.

Slip is modelled by solving (22) for all values of $[S_v]_{i+1/2}^{n+1}$.

3.5 Solution procedure

The discrete conservation equations discussed above are non-linear and strongly coupled. They are solved simultaneously using Newton-Raphson iterations. This method iteratively updates the primary variable vector, x, to drive the imbalance in the residual equations (e.g. (7), (8), (16) and (22)) to zero using the following linear system:

$$\mathbf{J}\Delta x = -R. \tag{29}$$

Here $\mathbf{J}$ is the Jacobian matrix and R is the residual vector calculated using the discretised conservation equations. This linear system is solved for the update vector, Δx, representing the change in primary variables.

The Jacobian matrix is defined as

$$J_{ij} = \frac{\partial R_i}{\partial x_j} = \frac{R_i(x_j + dx_j) - R_i(x_j)}{dx_j}. \tag{30}$$

It describes how the discrete residual equations given in Section 3 change with respect to the primary variables. It is used to drive the convergence of the residual equations to zero for each time step and, if not calculated accurately, can result in slow or failed convergence and erroneous solutions. Our simulator calculates the Jacobian using finite differencing. This involves perturbing the primary variable x_j by a small amount dx_j (scaled to the size of the primary variable) and taking the forward difference, as shown in (30). This method can be prone to truncation and round-off errors. Decreasing the step size, dx_j, will reduce the truncation error, however, it will also increase the round-off error. The optimal size of dx_j is unknown and differs for each residual equation. For this reason, dx_j is estimated as $dx_j = 1\mathrm{E} - 6 \times (x_j + 1)$.

4. TEST PROBLEMS

A suite of test problems has been developed to ensure the simulator can model a range of operating conditions. It also provides a benchmark for the numerical performance of the simulator to check out future developments. A subset of these problems is discussed below. Problems 1 to 4 all feature transitions between liquid and two-phase conditions, while Problems 5 to 8 include transitions between two-phase and vapour conditions.

4.1 Problem 1: Single feed 300 °C liquid production

Problem 1 simulates flow from a hot, liquid reservoir into a well initialised with hydrostatic liquid pressure profile and a linear temperature profile varying from 30 - 200 °C. The wellbore and formation properties are given in Table 3 and

feed properties are given in Table 4, where PI is the productivity index of the feed.

Flow in the well is started by dropping the wellhead pressure from 9.5 bar to 4.29 bar. Flashing initially occurs deep in the well due to the influx of hot fluid. This forces a slug of warm liquid up the well and causes flashing at the wellhead. Flashing continues until the entire length of the well is two-phase.

Table 3: Problem 1 - wellbore and formation parameters

Inclination angle	0 °
Length	1000 m
Cement thermal conductivity	1.4 W °C^{-1} m^{-1}
Formation thermal conductivity	2.4 W °C^{-1} m^{-1}
Geothermal gradient	0.27 °C/m
Pipe diameter	0.2205 m above 660 m
	0.1594 m below 660 m
Cement diameter	0.314 m above 660 m
	0.1694 m below 660 m
Pipe roughness	4.5E-5 m above 660 m
	9.0E-5 m below 660 m

Table 4: Problem 1 - feed properties

PI [m^3]	Depth [m]	P bar]	T [°C]	S$_v$ [-]
1E-13	950 - 1000	100	300	0.0

4.2 Problem 2: Wellbore shut-in

Problem 2 simulates the rapid shut-in of a flowing geothermal well. Flow is stopped over a period of 60 seconds using a time-dependent, mass flow boundary condition. The wellbore and feed-zone parameters given in Tables 3 and 4 are used for this simulation.

4.3 Problem 3: Single-feed 198.5 °C liquid production

Problem 3 simulates production from a deep liquid reservoir. Flashing in the well begins at the wellhead and proceeds down to approximately 1200 m. This process evolves slowly. The wellbore and feed properties are given in Tables 5 and 6, respectively. For this problem, the feed mass flux is calculated using $q_{mass} = \alpha(P_{res} - P_{wb})/V$. The value of the lumped parameter α is given in Table 6. The well is initialised with a hydrostatic, all-water pressure profile.

Table 5: Problem 3 - wellbore and formation parameters

Inclination angle	0 °
Length	2133 m
Cement thermal conductivity	1.4 W °C^{-1} m^{-1}
Formation thermal conductivity	2.4 W °C^{-1} m^{-1}
Pipe diameter	0.2215 m
Cement diameter	0.314 m
Pipe roughness	4.5E-5 m
Reservoir temperature	Figure 7 (Tonkin et al, 2020)

Table 6: Problem 3 - feed properties

α [kg s^{-1} Pa^{-1}]	Depth [m]	P[bar]	T [°C]	S$_v$ [-]
1.168E-6	2090 - 2140	210	198.5	0.0

4.4 Problem 4: Multi-feed liquid production

Problem 4 models the start-up processes of the example simulation given in Section 5 of Tonkin et al. (2020). It simulates production from a well with three liquid water feeds. The start-up processes are complex and feature internal flow from the shallow feed to the deeper feeds.

4.5 Problem 5: Single-feed vapour production

Problem 5 simulates the entire length of a wellbore transitioning from single-phase vapour to two-phase flow. This is achieved by transitioning the feed-zone from vapour to two phase conditions. The test well described in Table 3 is used in this problem and the feed-zone properties are given in Table 7. The formation temperature varies with time and is linear between $150 - T_{sat}(P_{feed})$°C, where P_{feed} is the transient feed pressure given in Table 7.

Table 7: Problem 5 - feed properties

Depth [m]	PI [m^3]	Time [days]	P [bar]	T [°C]	S$_v$ [-]
2090 - 2140	1E-12	242	20	300	1.0
		670	40	T_{sat}	1.0
		5895	40	T_{sat}	0.5

4.6 Problem 6: Multi-feed vapour production: flashing and condensing

Problem 6 tests transitions to and from single-phase vapour. The feed conditions, given in Table 8, vary rapidly and are designed to test the simulators ability to transition between two-phase and vapour conditions. The wellbore used in this simulation is 200 m deep with a constant diameter of 0.2205 m and a completion radius of 0.314 m. The formation temperature varies with time and is linear between $150 - T_{sat}(P_{feed})$°C, where P_{feed} is the transient pressure of the deep feed given in Table 8. The simulation is initialised with flowing vapour conditions.

Table 8: Problem 6 - feed properties

Depth [m]	PI [m^3]	Time [days]	P [bar]	T [°C]	S$_v$ [-]
950 - 1000	1E-12	0	20	T_{sat}	0.0
		9	20	T_{sat}	1.0
		36-59	20	300	1.0
		70	20	T_{sat}	1.0
		82	20	T_{sat}	0.0
400 - 450	1E-12	constant	20	300	1.0

4.7 Problem 7: Multi-feed vapour production: transient deep feed

Problem 7 builds on Problem 5 by adding a shallow vapour feed. The deep feed-zone slowly transitions from vapour conditions to two-phase conditions as given in Table 9. This causes the well to condense to two-phase conditions below the shallow feed, while above, the well remains single phase vapour.

This problem uses the test well given in Table 3. It is a vertical 1000 m well with a change of internal diameter, from 0.2205

m to 0.1594 m, at a depth of 660 m. It is initialised with flowing vapour conditions and uses the transient formation temperatures from Problem 5.

Table 9: Problem 7 - feed properties

Depth [m]	PI [m³]	Time [days]	P [bar]	T [°C]	S_v [-]
950 - 1000	1E-12	242	20	300	1.0
		670	40	T_{sat}	1.0
		6242	40	T_{sat}	0.5
400 - 450	1E-12	constant	20	300	1.0

4.8 Problem 8: Multi-feed vapour production: transient shallow feed

Problem 8 is identical to Problem 7, except that in this case it is the shallow feed that transitions to two-phase conditions, as specified in Table 10. This causes the top of the well to transition to two-phase conditions above the shallow feed while the rest of the well remains in single-phase conditions. The transient formation temperatures from problem 5 are used.

Table 10: Problem 8 - feed properties

Depth [m]	PI [m³]	Time [days]	P [bar]	T [°C]	S_v [-]
950 - 1000	1E-12	242	20	300	1.0
		670	40	T_{sat}	1.0
		6242	40	T_{sat}	0.5
400 - 450	1E-12	constant	20	300	1.0

5. RESULTS AND DISCUSSION

The performance of the primary variable formulations is compared using three metrics. These are the total number of time steps, linear solves, and equation of state (EOS) errors that occur during a simulation. EOS errors include cases when primary variables step outside of thermodynamic bounds and errors caused by upwinding (e.g. when $[S_v\rho_v]_{i+1/2}^{n+1} + [S_l\rho_l]_{i+1/2}^{n+1} = 0$).

Simulations with liquid transitions (problems 1 to 4) are discussed in Section 5.1 while simulations with vapour transitions (problems 5 to 8) are discussed in Section 5.2.

5.1 Liquid transition results

Figures 3 a) and 3 b) show that in all test cases with liquid transitions the velocity formulation performs significantly better than the volume flux formulation. The performance of the mixed formulation is slightly better than the velocity formulation. Figure 3 c) shows the number of EOS errors are similar for all formulations.

Problem 3 shows the greatest difference between methods. The volume flux method takes 567 time steps and 1938 linear solves compared to 177 time steps and 288 linear solves taken by the mixed method. This poor performance can be explained by considering the gradient of the constitutive slip equation (4) with respect to the vapour volume flux. When $S_v \approx 0$,

$$\frac{\partial}{\partial F_{Vv}}\left(\frac{F_{Vv}}{S_v} - (F_{Vv} + F_{Vl}) - u_d\right) = \frac{1}{S_v} - 1 - \frac{\partial u_d}{\partial F_{Vv}} \approx \frac{1}{S_v}. \quad (31)$$
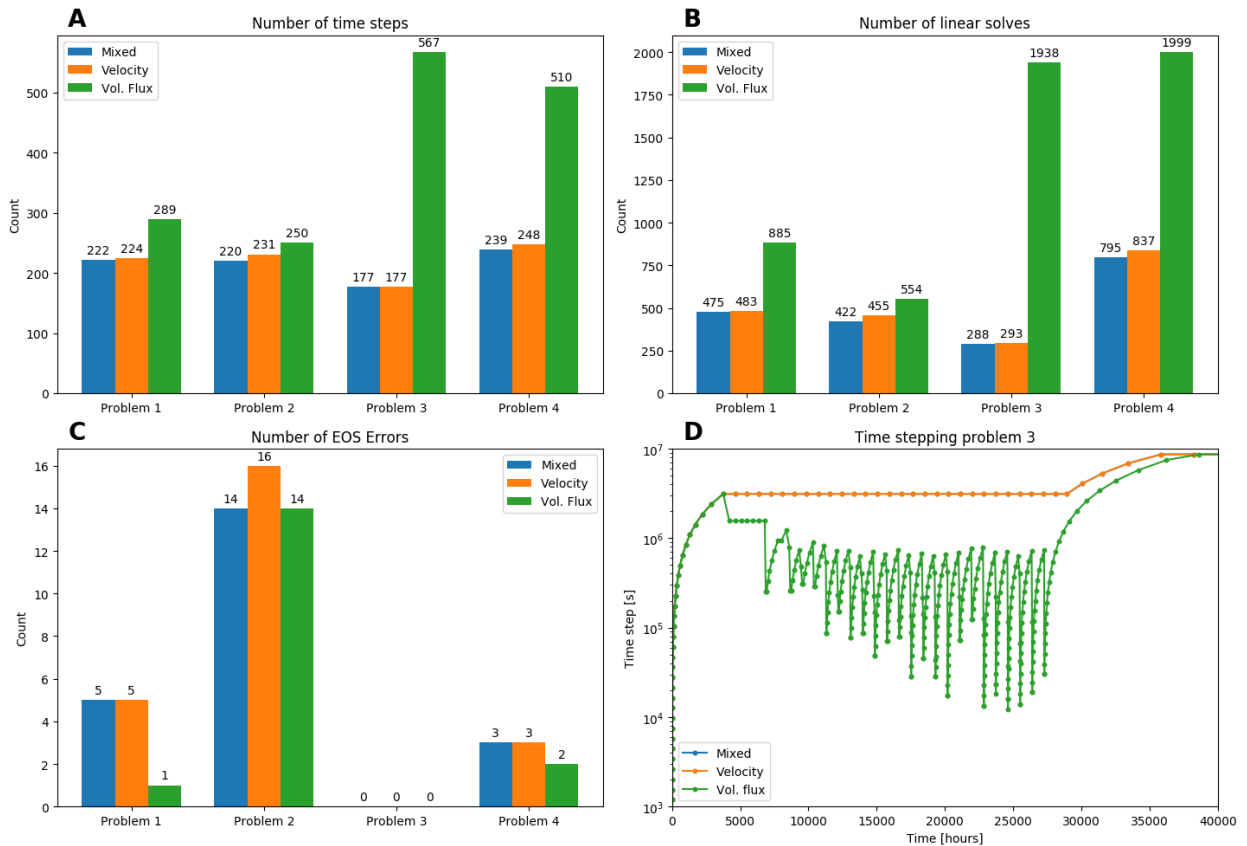

Figure 3: Comparison of the total number of A) time steps B) linear solves and C) EOS errors for Problems 1 – 4. A comparison of the time stepping for Problem 3 is given in D).

This gradient is large compared to the magnitude of (4) meaning small changes in the vapour flux result in large changes in the residual equation and inaccurate updates of primary variable are calculated. As a result, the simulation is only stable if one element flashes per time step as evident in the cyclical time stepping shown for Problem 3 in Figure 3 d).

5.2 Vapour transition results

Figures 4 a) and 4 b) show the total number of time steps and linear solves taken for Problems 5 to 8. They indicate that, for cases with vapour transitions, the volume flux formulation performs significantly better than the velocity formulation. In all cases, volume flux requires fewer time steps and fewer linear solves. The performance of the mixed formulation is identical to that of the volume flux formulation.

The poor performance of the velocity formulation is highlighted by the time stepping comparison for Problem 7 given in Figure 4 d). Here, the velocity method drops the time step every time an element condenses. Comparatively, the volume flux and mixed formulations allow the entire bottom section of the well to condense in a single time step.

The worst performance of the velocity formulation is for problem 8. Here, the run was stopped after 5800 timesteps. At this point it had completed over 33,900 linear solves but was less than halfway through the simulation. By comparison, the volume flux and mixed formulations required only 83 time steps and 184 linear solves. This poor performance makes the

velocity formulation unusable for many high saturation problems.

It should also be noted that the velocity formulation cannot simulate Problems 5 to 8 without switching the slip equation for high saturations as was described in Section 3.2. This can be explained by considering the derivatives of the constitutive slip equation.

Assuming $C_0 = 1$, the derivatives of (4), in residual form, with respect to the liquid and vapour velocities, are

$$\frac{\partial}{\partial u_v}(u_v - (S_v u_v + S_l u_l) - u_d) = 1 - S_v - \frac{\partial u_d}{\partial u_v}, \quad (32)$$

and

$$\frac{\partial}{\partial u_l}(u_v - (S_v u_v + S_l u_l) - u_d) = -S_l - \frac{\partial u_d}{\partial u_l}. \quad (33)$$

When $S_v \approx 1$, such is the case when an element transitions to or from vapour flow, $\partial u_d / \partial u_\beta \approx 0$. Note that this may not be the case if other empirical equations for u_d are used. Given this, it is clear from (32) and (33) that

$$\frac{\partial}{\partial u_v}(u_v - (S_v u_v + S_l u_l) - u_d) \approx 1 - S_v \approx 0, \quad (34)$$

and

$$\frac{\partial}{\partial u_l}(u_v - (S_v u_v + S_l u_l) - u_d) \approx -S_l \approx 0. \quad (35)$$
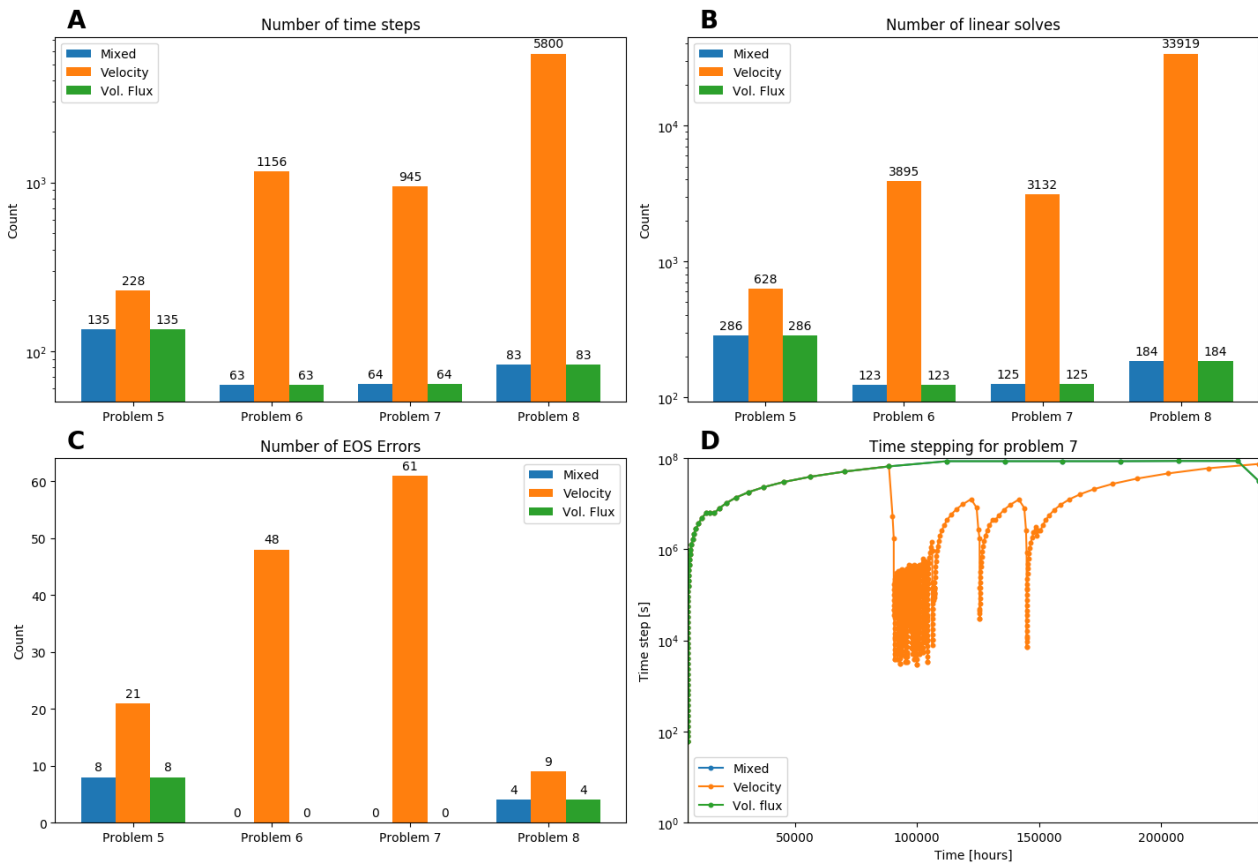

Figure 4: Comparison of the total number of A) time steps B) linear solves and C) EOS errors for Problems 5 – 8. A comparison of the time stepping for Problem 7 is given in D).

These gradients result in a near singular Jacobian, bad primary variable updates and, ultimately, the failure of the simulation. Equation (5) is used for simulations where $S_v \approx 1$ for this reason. Assuming $C_0 = 1$, the derivatives of (5) with respect to the vapour velocity is

$$\frac{\partial}{\partial u_v}\left(u_l - (S_v u_v + S_l u_l) + \frac{S_v}{1-S_v}u_d\right) =$$

$$-S_v + \frac{S_v}{1-S_v}\frac{\partial u_d}{\partial u_v} \approx -1 + \frac{1}{1-S_v}\frac{\partial u_d}{\partial u_v}. \quad (36)$$

The derivative with respect to liquid velocity is

$$\frac{\partial}{\partial u_l}\left(u_l - (S_v u_v + S_l u_l) + \frac{S_v}{1-S_v}u_d\right) =$$

$$1 - S_l + \frac{S_v}{1-S_v}\frac{\partial u_d}{\partial u_l} \approx 1 + \frac{1}{1-S_v}\frac{\partial u_d}{\partial u_l}. \quad (37)$$

These gradients are non-zero and do not result in a singular Jacobean. However, the velocity code still shows poor convergence and the high number of EOS errors in Problems 2 and 3 as shown in Figure 4 c). This indicates that the primary variables are frequently stepping outside of their thermodynamic bounds which suggests there are bad gradients in the Jacobian. The gradient of (5) with respect to vapour saturation is,

$$\frac{\partial}{\partial S_v}\left(u_l - (S_v u_v + S_l u_l) + \frac{S_v}{1-S_v}u_d\right)$$

$$= +u_l - u_v + \frac{u_d}{(1-S_v)^2} + \frac{S_v}{1-S_v}\frac{\partial u_d}{\partial S_v}. \quad (38)$$

As $(1 - S_v) \lesssim 1E-7$ when transitioning to and from vapour, the gradient given by (38) is very large which causes bad primary variable updates and poor convergence. Limiting the size of S_v, as is done in (24), reduces, but does not prevent, this issue.

Using the mixed formulation avoids all the issues discussed above. When vapour saturation is low, the gradient given in (31) is avoided and when vapour saturation is high the issues discussed with (34) to (38) are avoided. The mixed formulation has the best performance as a result.

The discussion above indicates that the form of the slip equation has a large impact on the performance of different primary variables and the simulators ability to transition between phase states. Analysis similar to the above can help guide the choice of flowing primary variables when implementing different slip relationships. For example, if the relative velocity equation, $u_r = u_v - u_l$, is used the velocity formulation would perform well for all cases whereas the volume flux variables would perform poorly at both high and low saturations.

6. CONCLUSION

This work presents the numerical implementation of a new transient geothermal wellbore simulator capable of modelling two-phase flow in complex wellbores. The discrete conservation equations and the constitutive equation for slip were solved implicitly for four primary variables. It was found that using both phase velocities as primary variables resulted in poor performance for cases with high vapour saturation. Similarly, it was found that using both phase volume fluxes resulted in poor performance for cases with low vapour saturation. The best choice of primary variables,

of those tested, was the mixed formulation (P, $T(S_v)$, u_v and F_{Vl}). It performed at least as well as the other formulations on all problems. The poor performance of the velocity and volume flux formulations was explained by considering the analytical gradients of the constitutive slip equation with respect to the primary variables. This method can be used to help determine whether a primary variable is appropriate for different slip models.

REFERENCES

Akbar, S., Fathianpour, N. and Al-Khoury, R.: A finite element model for high enthalpy two-phase flow in geothermal wellbores, *Renewable Energy*, 94. pp. 223–236. (2016).

Croucher, A. Waiwera User's Guide (1.2.1). (2020).

García-Valladares, O., Sánchez-Upton, P. and Santoyo, E.: Numerical modeling of flow processes inside geothermal wells: An approach for predicting production characteristics with uncertainties, *Energy Conversion and Management*. pp. 1621-1643. (2006).

Miller, C.: *Wellbore User's Manual*, University of California, Berkeley, CA. (1980).

Pan, L. and Oldenburg, C. M.: T2Well - An integrated wellbore-reservoir simulator, *Computers and Geosciences*, 65. pp. 46–55. (2014).

Pan, L., Webb, S. W. and Oldenburg, C. M.: Analytical solution for two-phase flow in a wellbore using the drift-flux model, *Advances in Water Resources*, 34. pp. 1656–1665. (2011).

Pruess, K., Oldenburg, C. M., & Moridis, G. TOUGH2 User's Guide (No. 2). (2012).

Shi, H. Holmes, J., Durlofsky, L., Aziz, K., Diaz, L., Alkaya, B and Oddie, G.: Drift-Flux Modeling of Two-Phase Flow in Wellbores, *SPE Journal*. Society of Petroleum Engineers, 10. pp. 24–33. (2005).

Tachimori, M. A Numerical Simulation Model for Vertical Flow in Geothermal Wells. Proc, 8th Workshop Geothermal Reservoir Engineering Stanford University, Stanford, CA. (1982)

Tonkin, R. O'Sullivan, J. and O'Sullivan, M. Development of a transient, multi-feed geothermal wellbore simulator. Proc. 42nd New Zealand Geothermal Workshop, Waitangi, NZ. (2020).

Yadigaroglu, G., & Hewitt, G. F. (2018). Introduction to Multiphase Flow (G. Yadigaroglu & G. F. Hewitt (eds.)).

Zuber, N. and Findlay, J. A.: Average Volumetric Concentration in Two-Phase Flow Systems, *Journal of Heat Transfer*. ASME, 87. pp. 453–468. (1965)